Spatiotemporal structure of hydrothermal waves in Marangoni convection

A. B. Ezersky,* A. Garcimartín,† H. L. Mancini,‡ and C. Pérez-García§
Departamento de Física y Matemática Aplicada, Facultad de Ciencias, Universidad de Navarra, 31080 Pamplona, Navarra, Spain
(Received 24 May 1993)

When a liquid layer is laterally heated, the basic flow loses stability in the form of hydrothermal waves. They can be visualized by means of the shadowgraph technique. The characteristics of these waves are studied by performing the Fourier transform on a spatiotemporal diagram. The frequency and the wave number inside the range of instability are studied, and the corresponding dispersion relation is determined. Some other two-dimensional features of the waves have also been observed, such as the dependence of the wave-front shape on the thermal characteristics of the lateral walls. Finally, a Ginzburg-Landau equation is proposed to describe these waves, and several coefficients in this equation are estimated from the experimental data.

PACS number(s): 47.35.+i, 47.20.Dr

I. INTRODUCTION

The investigation of propagative patterns in far-from-equilibrium systems has attracted considerable attention in recent years [1]. Such patterns appear in many different situations, for example, in hydrodynamic instabilities, lasers, chemical reactions, etc. Moreover, they may be regarded as a first state in the transition to spatiotemporal complexity and to turbulence in those systems. The characterization of hydrothermal waves is also interesting because they appear in crystal growth when using the floating-zone method [2] and are important for the transport of impurities and mixing processes.

In a previous paper [3] we showed experimentally the existence of hydrothermal waves in a nonhomogeneously heated device. Measurements of the threshold of these waves and their characteristic frequency, wave number, and velocity of propagation were carried out in a cylindrical liquid layer.

In these experiments some indications showed that the waves could also be observed in a system with lateral heating. Here we report further experiments on the spatio-temporal evolution of these waves in a laterally heated container. Wave formation is preceded by a global circulation between the cold and the hot regions, called return flow [see Fig. 1(a)], with a velocity proportional to the lateral temperature gradient, which completely fills the container (zero wave number). This system has therefore some of the features of open flows: the waves are entrained by the global flow. When the temperature gradient exceeds a certain threshold, spontaneous hydrothermal waves traveling downstream can be observed. Schwabe *et al.* [4] have studied surface waves at large Marangoni numbers ($\mathrm{Ma}\approx 10^4$) in cavities of different shapes, but they only report waves traveling azimuthally near the heater. These waves seem to be the so-called surface waves, described by Smith and Davis [5,6]. Another form of secondary instability concerning

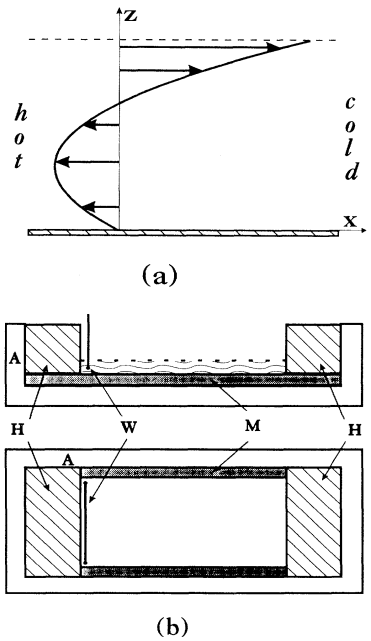

FIG. 1. (a) Sketch of the basic return flow (after [5]) in the middle of the cavity, showing the choice of coordinates. The analytical solution is $v_z = 0.75z^2 - 0.5z$. The waves travel from the hot end to the cold end. (b) Sketch of the cavity. *A*, adiabatic walls; *H*, copper heaters, *M*, metal bottom and walls; *W*, Nichrome wire. In some runs, piece *M* was changed for another made of Plexiglas.

*Permanent address: Institute for Applied Physics, Russian Academy of Sciences, Nizhny Novgorod, Russia.
†Author to whom all the correspondence should be addressed. Electronic address: cape@cpd.unav.es
‡Also at CITEFA/CONICET (1603 Villa Martelli) and Universidad de San Luis, Chacabuco y Pedernera, 5700 San Luis, Argentina.
§Also at Departament de Física Fonamental, Facultat de Física, Universitat de Barcelona, Avgda. Diagonal 647, 08028 Barcelona, Catalonia, Spain.

surface waves in a different (quasi-one-dimensional) geometry has been studied recently [7].

One important question at this point is whether the appearance of waves is the result of absolute or convective instability [8]. When waves propagate in a boundary layer or on an inclined plane their amplitude grows down the flow. Such flows can be considered to be distributed disturbance amplifiers and near the threshold the instability has a convective nature. The velocity field is confined by lateral walls and mass transport in every cross section is equal to zero. In such a situation it is not obvious that propagative waves, even near the threshold, should appear as a result of convective rather than absolute instability. To check this point we studied the evolution of artificially imposed perturbations on the basic flow and examined their development. Such an approach is quite common for investigating hydrodynamic instabilities. Experiments with external perturbations are made for Tollmien-Schlichting waves in boundary layers [9] and more recently for surface waves in a film falling down an inclined plane [10]. Thus the main aim of the present work can be summarized as the description of the spatiotemporal organization of the hydrothermal waves.

The outline of the paper is as follows. Experimental procedure and data processing techniques are described in Sec. II. In Sec. III the spatiotemporal behavior of the waves is presented as observed in the experiments. We discuss our results and draw a comparison with theoretical models in Sec. IV.

II. EXPERIMENTAL PROCEDURE

In the experiment we intend to set the conditions close to the assumptions for which theoretical studies of instabilities in laterally heated containers predict propagating waves [5,6]. We therefore use a long channel wide enough for the basic return flow [see Fig. 1(a)] to be two dimensional in the central part. The inner dimensions of this rectangular container are 5×7 cm^2 while the typical wavelength is about 5 mm. This setup makes it possible to investigate geometrical features of the waves, such as the shape of the wave fronts. (In the circular geometry we used before [3] that information was hidden by the cylindrical divergence of the waves.) We carried out the experiments described here in two different kinds of containers. One type is made of Plexiglas walls (which can be considered adiabatic) and a transparent insulating bottom. The other type of container is made of metal, and so both the walls and the bottom are good thermal conductors. Two copper heaters are placed at the two ends of the container as shown in Fig. 1(b). The temperature at each end is set by water coming from two thermal baths that is made to circulate inside the copper heaters, where the temperature is stabilized within 0.1 °C.

The liquid we use is 5 cSt silicon oil, its relevant properties being listed in [3]. For most purposes the Prandtl number Pr can be considered infinite. In different runs we experimented with depths ranging from 1.2 to 3.1 mm. Near the walls a meniscus forms and so the observation must be restricted to the central part of the cavity, to a zone of about 3×5 cm^2.

To introduce a perturbation we use a periodically heated Nichrome wire [Fig. 1(b)]. This wire is submerged in the liquid and stretched between two holders that keep it straight even when heated. It was leveled parallel to the bottom and placed close to the hot end of the cavity. The wire diameter is 0.12 mm and its electrical resistance is 2.4 Ω. We apply to it a sinusoidal current to obtain periodic thermal perturbation in the lateral heating by the Joule effect.

To visualize the hydrothermal waves we use the shadowgraph technique described elsewhere [3,11]. When we investigate the waves in the Plexiglas cavity we place a mirror under the transparent bottom. In this case the image contrast is due to the propagation of light through a liquid where temperature fluctuations exist. These are large enough to allow good image processing. To observe the waves in the metallic cavities the reflection from the surface is collected. Small surface deflections are visible as bright and dark regions depending on whether they are concave or convex. The image and data processing system consists of a standard charge-coupled-device (CCD) camera and a video recorder connected to a computer.

Before describing the experimental results we will briefly explain how to relate the contrast of the shadowgraph to some characteristics of the hydrothermal waves. Suppose that we have a liquid layer with temperature disturbances in the form of traveling waves:

$$T(x,z,t)=A(x,t)\tilde{T}(z)\cos(\omega t-kx)\ , \tag{1}$$

where z stands for the vertical coordinate inside the liquid layer and x for the coordinate down the flow, ω is te frequency, and k is the wave number of the waves. $A(x,t)$ is the slowly varying amplitude.

Now consider a light beam propagating perpendicularly to the liquid surface and reflecting in a mirror at the bottom of the cavity. If we neglect the reflection from the surface, the intensity of the light beam passing through the liquid and reflected from the bottom may be written as [11]

$$\frac{\Delta I}{I}=2d\int_0^d\frac{\partial^2}{\partial x^2}\ln(n)dz\ . \tag{2}$$

Here d is the depth of the layer and n is the refractive index, which in first approximation depends on temperature disturbances as

$$n=n_0+\alpha T\ . \tag{3}$$

For small temperature fluctuations we have

$$\frac{\Delta I}{I}=-2d\alpha Ak^2\cos(\omega t-kx)\int_0^d\frac{1}{n_0}\tilde{T}\,dz\ . \tag{4}$$

Thus the intensity variations of the shadowgraph are proportional to the temperature fluctuations, averaged over the depth. From (4) it can be seen that the main characteristics of the waves can be obtained from these variations.

III. EXPERIMENTAL RESULTS

For sufficiently small temperature differences a single convective cell with streamlines going from the heating

end to the colder one and back [Fig. 1(a)] can be observed. This is the so-called return flow. For a larger temperature difference some waves begin to propagate superimposed on the return flow. A shadowgraph picture for a liquid depth $d=3.1$ mm is shown in Fig. 2. The temperature at the hot end of the cavity is $T=67$°C and at the cold end it is $T=41$ °C. In this experiment we have not covered the whole range of parameters (depth, temperature difference) explored in our previous work [3], but we can assert that for the values in this experiment the temperature threshold and the frequency are roughly the same. Moreover, there is no reason to think that the characteristics of hydrothermal waves should change with geometry in large-aspect-ratio experiments. From Fig. 2 one can notice that these waves appear clearly at some distance from the hot wall and they disappear before reaching the cold side. The wave fronts are not regular and some defects are visible. The first fact suggests that perturbations grow near the hot end and saturate downflow. The second feature is probably due to the fact that the wave is not generated in phase along the heating wall. It should be noted that this instability is very different to the Bénard-Marangoni convection (which appears when a liquid layer is heated from below) in which, for the type of liquid used in these experiments, stationary hexagonal cells would be obtained. It is also different from convection in vertical layers [12]. The problem we are dealing with combines lateral heating instability and the Marangoni effect. On one hand, the sidewall heating induces a destabilization of the lateral thermal boundary layer, giving rise to the convective cell that sets up the return flow. On the other hand, the surface tension variations are responsible for the destabilization of the interface, reinforcing the return flow, and making surface motions possible. However, as stressed in a previous article [3] the nature of the waves observed in this system is not yet well established.

Hydrothermal waves grow naturally in the system.

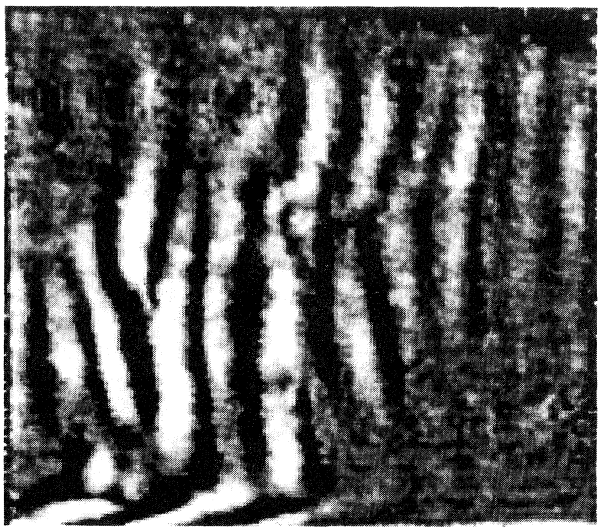

FIG. 2. Shadowgraph of hydrothermal waves. The image covers only a zone of the cavity of 3.7×3.2 cm^2.

The relevant dimensionless parameter is the horizontal Marangoni number, defined as

$$\mathrm{Ma}=\frac{\dfrac{d\sigma}{dT}\dfrac{T_1-T_2}{l}d^2\mathrm{Pr}\rho}{\mu^2}\ . \tag{5}$$

Here $d\sigma/dT$ is the coefficient of variation of surface tension with temperature, l is the length between the hot and cold sides, μ is the viscosity of the liquid, Pr is the Prandtl number, and ρ is the oil density. In our experiment, the Marangoni number turns out to be typically $\mathrm{Ma}\simeq1200$.

To improve the coherence of the waves we artificially perturb the basic flow with periodic heating as described in Sec. II. The spatial structure (Fig. 3) becomes more regular, almost without defects. These shadowgraphs correspond to a perturbation frequency $f_0=1.7$ Hz and an amplitude $V=0.3$ V.

It is possible to obtain information on the behavior of the wave amplitude along the flow by performing a Fourier transform. This is done in the following way. A line of pixels parallel to the basic flow (x direction) and close to the center of the cell is recorded at regular time intervals (typically 0.1 s) and stacked, thus giving an x-t diagram such as the one shown in Fig. 4. Waves appear as dark and bright stripes of nearly constant velocity. From this image vertical lines ($x=$const) are taken at regular space intervals (typically 1 mm) and the power spectrum of each line is calculated. To reduce the noise, the background brightness is subtracted and the lines are windowed. (Instead of calculating the Fourier transform of a whole line, the fast Fourier transform of a portion, or window, of the line is carried out. Then the window is moved, and after sweeping the whole line the resulting power spectra are averaged.) The Fourier transforms are then displayed in a three-dimensional graph (Fig. 5) where the power is plotted versus frequency and distance along the container. We have also used the same method to investigate the behavior of the wave number, in this case by computing the Fourier transform of horizontal lines ($t=$const).

It can be seen in Fig. 5(a) that the instability range spans from 1 to 2 Hz. At the beginning of the flow high-frequency fluctuations predominate; down the flow low-frequencies dominate and at the end of flow all disturbances decay. By means of the heating wire, a perturbation with a frequency f_0 inside or close to the range of instability in introduced and its behavior downflow is examined. In Fig. 5(b) we show a typical picture obtained for a forcing frequency within the range of instability. Near the wire only a decrease in perturbations is observed. This decrease can be explained as follows. When heating the wire with a sinusoidal current, periodically heated regions are created in the flow. These disturbances are not eigenmodes of the flow and decay, but they transfer their energy to unstable modes that grow downflow.

Cross sections of the spectra $S(x,f_0)$ are shown in Fig. 6. The amplitude of the external forcing was the same for all frequencies. It can be seen that there is an increase of amplitude only in the first third of the cavity. In an in-

termediate region the amplitude of the instability seems to saturate. Near the cold wall the waves disappear. We performed some control experiments to determine the origin of these effects. First, the external forcing amplitude is increased. The dependence of amplitude on x for different amplitudes of excitation ($V=0.3$, 0.5, and 0.7 V) is shown in Fig. 7. Second, we measured the temperature distribution along the flow. Five thermocouples are introduced on the bottom near the middle of the cavity. The distribution of temperature is shown in Fig. 7. In the first third of the cavity we have a large temperature gradient. Therefore, Ma is not uniform, but varies downflow: it is approximately linear and positive only near the heating wall. [If we recalculate Eq. (5), the local value of the Marangoni number in that region is about 3 times greater than the average.] It is in this region where we observe an amplification of temperature perturbations. Near the cooling wall the temperature gradient decreases. This means that the observed behavior of the amplitude is connected with temperature profile and the fact that Ma(x) decreases downflow.

The evolution of the waves strongly depends on the applied perturbation frequencies. When a perturbation with a frequency close to the left edge of instability is applied, some peaks appear in the spectra wave at the right of f_0. For frequencies close to the right edge, the peaks appear at the left of f_0 [see Fig. 5(b)]. Frequencies close to the center of the instability range lead to the suppression of other frequencies [Fig. 5(c)]. An increase in the amplitude of excitation leads to still more suppression [Fig. 5(d)]. In our opinion, this is the displaying of nonlinear wave competition. The appearance of such peaks [Figs. 5(b) and 5(c)] means that energy is being transferred from the disturbances to modes with a larger temporal growth factor. If this process takes place in

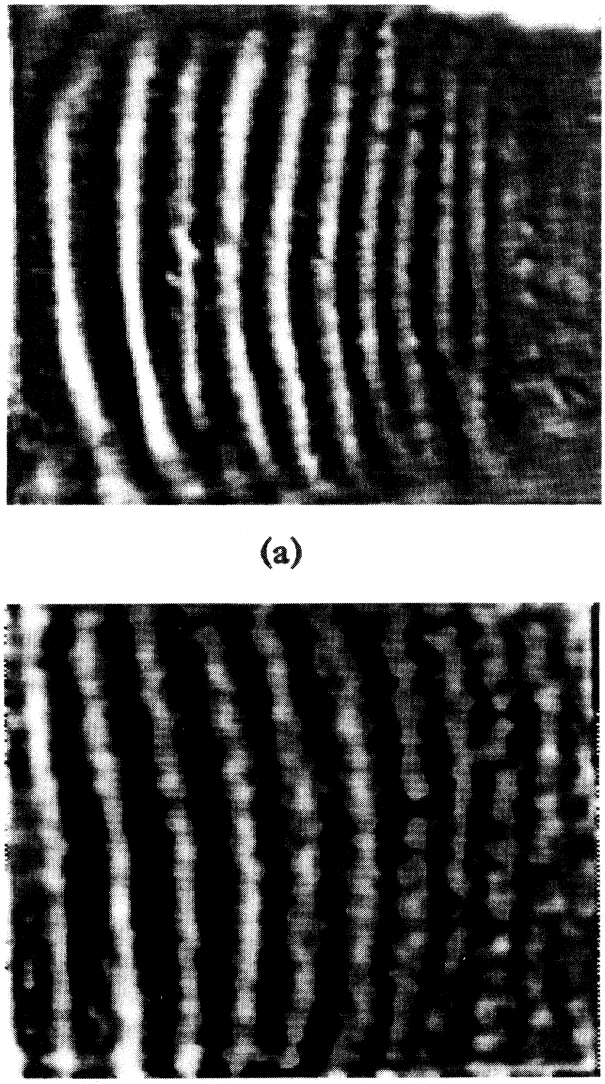

FIG. 3. Hydrothermal waves with external excitation (a) in a Plexiglas cavity and (b) in a metal cavity. The perturbation is a pulse of frequency $f_0=1.7$ Hz and $V=0.3$ V. Both images display the same zone as in Fig. 2.

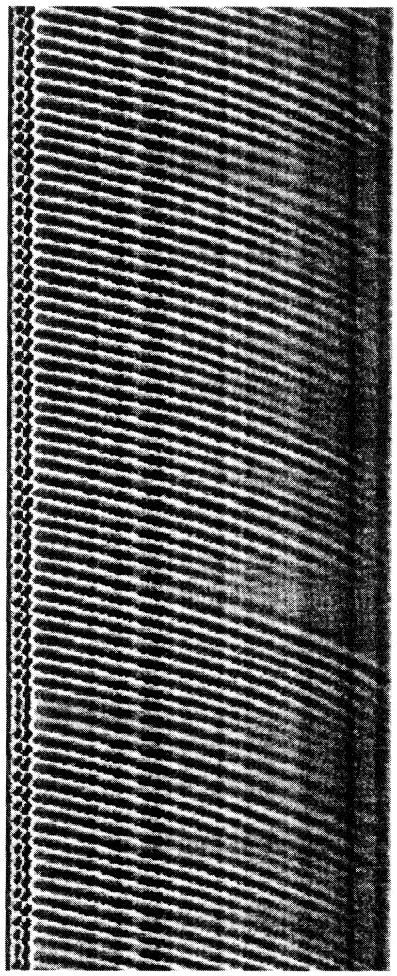

FIG. 4. x-t diagram obtained by recording a line of the shadowgraph image over a certain time. The horizontal axis is 3.5 cm long and the vertical axis covers 51.2 sec.

space instead of time it is called Eckhaus instability [13].

To determine the dependence of frequency on the wave number, we have compared the oscillation phase at different points along the flow by calculating the cross correlations of the time series (which are vertical lines in the x-t diagrams) at different positions. Before performing the cross correlations we filtered the time series by only keeping a frequency range of approximation $f_0 \pm 10\%$. If we make a best fit approximation in the form

$$\omega = \omega_0 + Vk + Bk^2 , \tag{6}$$

we can estimate the group velocity and the dispersion parameter for propagating waves. Results of these calculations are shown in Fig. 8.

The wave number k, however, is not constant downstream. As was shown above, we have a nonlinear profile of temperature (Fig. 7) and flow velocity and accordingly wave velocities decreases downflow. As long as frequency is conserved in the steady spatial nonhomogeneous situation, wave number increases downflow.

To obtain a more linear temperature distribution along the flow, in other runs we used a metal cavity. We established that temperature distribution was much more linear than in the case of adiabatic walls. Propagating waves have approximately the same properties as in the previous case. The main difference between the two series of experiments was the following. For adiabatic walls, wave fronts were curved with the concavity directed downstream. Wave fronts in the metallic cavity were also curved, but the concavity was directed upstream [Fig. 3(b)]. This may be connected with the thermal conductivity of the walls. In other words, the angle between the wall and wave front seems to depend on the thermal conductivity of the walls.

To check this conjecture we carried out some runs with one metal wall and one Plexiglas wall. The structure of wave fronts is presented in Fig. 9. Wave fronts were inclined and the angles of inclination near the upper wall (metal) and the lower wall (Plexiglas) coincide with the inclination of wave fronts in all-metal and all-Plexiglas cavities.

Two points should be emphasized. First, the shadowgraph is very sensitive to different disturbances such as air motion, air bubbles inside the silicon oil, contamination, and so on. When such disturbances affected the experiment the picture of waves became very complicated and it was impossible to find any simple configuration

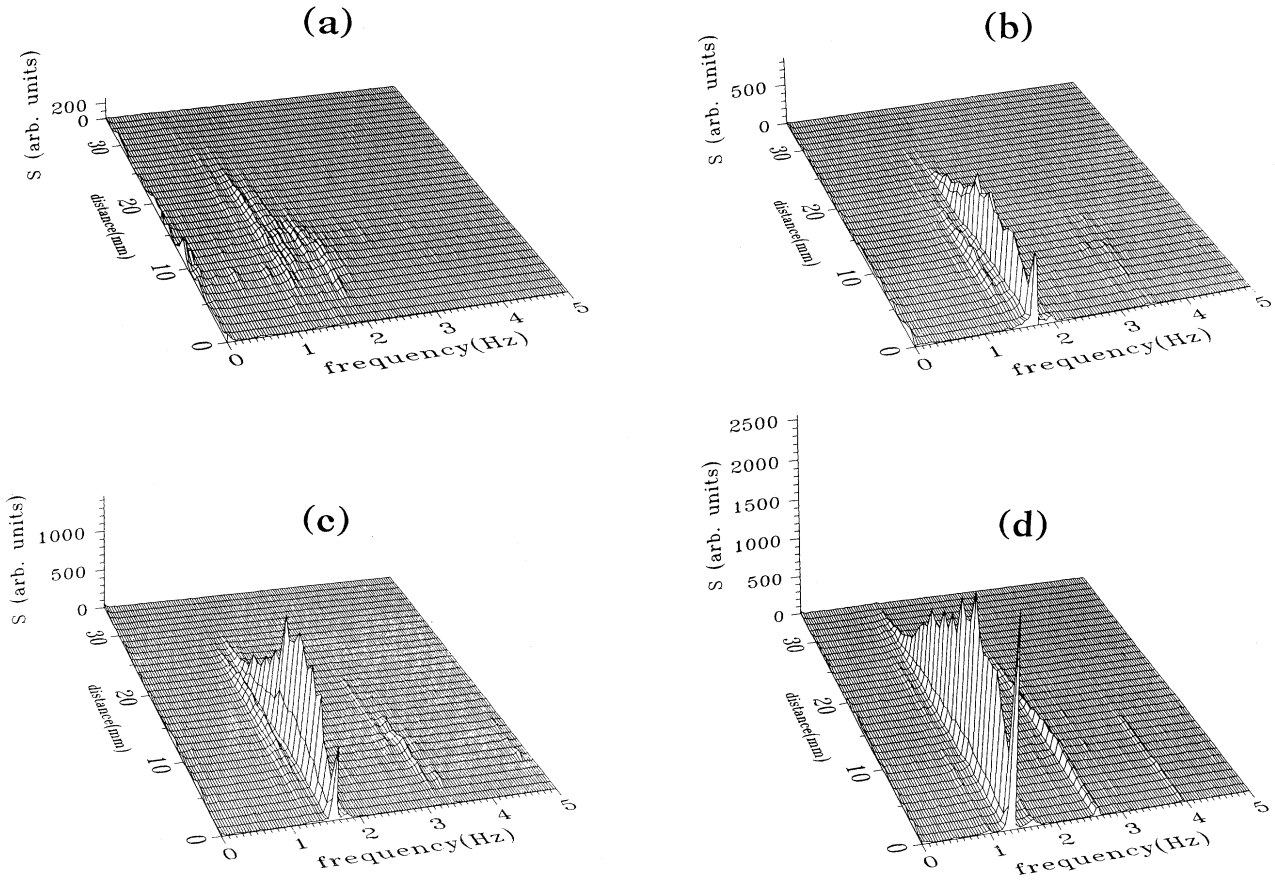

FIG. 5. Power spectral density (S) along the flow (a) without external excitation, Ma$\simeq$1200; (b) with external excitation $f_0 = 1.7$ Hz and $V = 0.3$ V; (c) $f_{0-} = 1.6$ Hz and $V = 0.3$ V; and (d) $f_0 = 1.3$ Hz and $V = 0.5$ V. All the graphs are drawn to the same scale.

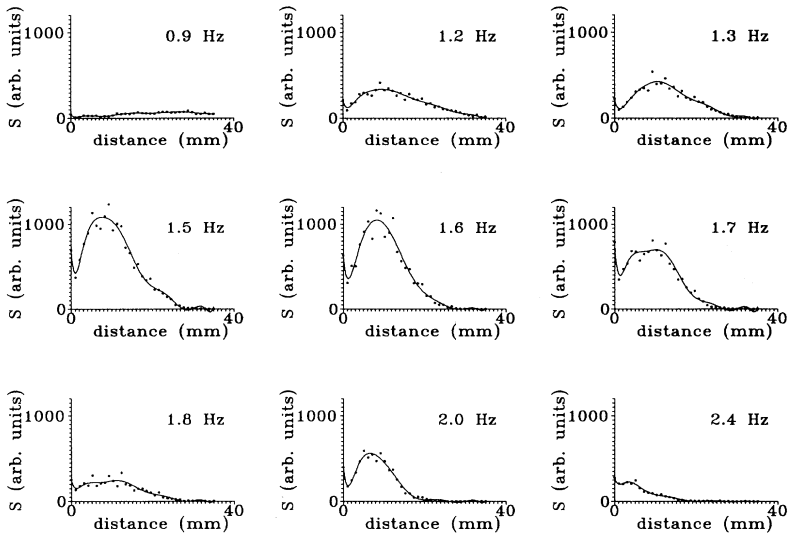

FIG. 6. Cross sections of the power spectral density (S). The cross sections were taken at the frequency of excitation for an amplitude $V=0.3$ V. All the graphs are drawn to the same scale.

such as we describe above. But three types of wave front may be considered to be the preferred configurations under definite boundary conditions and in the absence of external disturbances. Second, the different inclination of fronts is not connected with the meniscus formed near the walls because the contact angle of the silicon oil is similar for both materials.

IV. COMPARISON WITH SOME THEORETICAL MODELS

Smith and Davis [5,6] considered propagating waves of two possible origins in a laterally heated liquid, namely those arising from hydrothermal instability (hydrothermal waves) and those coming from capillary deformations (surface waves). The physical mechanism responsible for these two instabilities is very different. Surface waves arise from a shear instability of the velocity field. If the return flow were established without a temperature field, surface waves would nevertheless be present. Thus the temperature gradient is only relevant in setting the fluid in motion. Hydrothermal waves, on the other hand, have a thermal origin. If we assume that a disturbance creates a hot line in the surface perpendicular to the flow direction, a net force arises due to the variation of surface tension with temperature. As for most liquids, surface tension decreases with temperature (and indeed, this is the case for silicon oil), this force would drag the hot line towards the colder zone. The same could be said if the hot line were created below the surface, because buoyancy would then establish a local closed circulation that would result in an increase in the surface temperature above the disturbance, and the hot

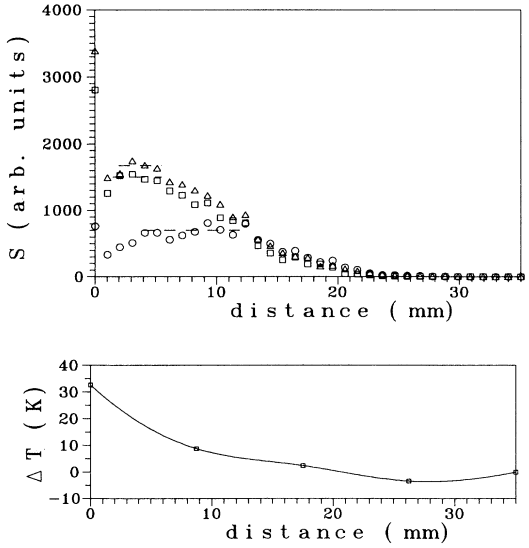

FIG. 7. Cross sections of the power spectral density (S) for different amplitudes of excitation (0.3, 0.5, and 0.7 V) and $f_0=1.7$ Hz (top) and the temperature difference—taking as reference the cold end—along the bottom of the cavity (bottom).

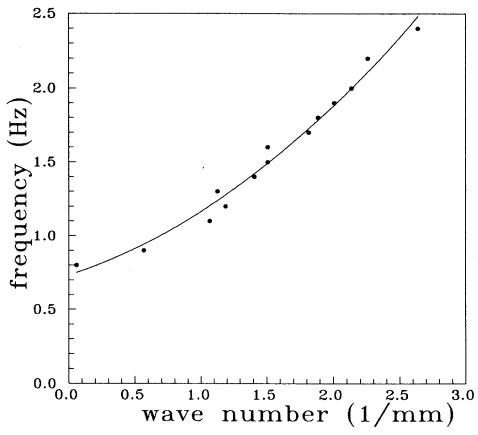

FIG. 8. Frequency vs wave number for Ma$\simeq$1200. The fit is $f=0.73+0.29k+0.14k^2$.

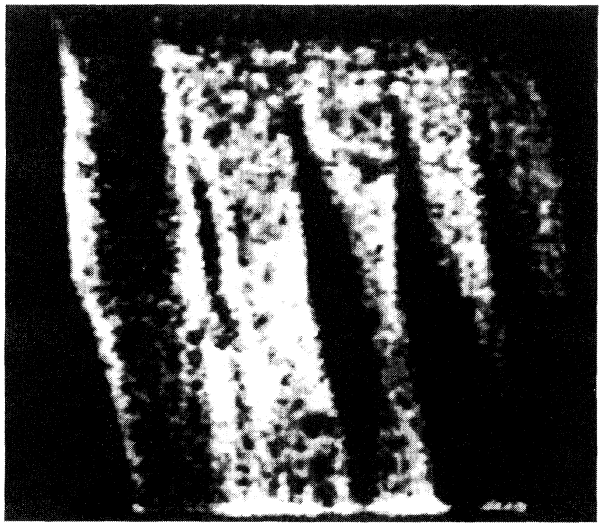

FIG. 9. Shadowgraph of hydrothermal waves in a cavity with one metal wall and one wall of Plexiglas. The area covered by the photograph is 3.7×3.2 cm^2.

line would be carried away as well. The temperature gradient is thus necessary for hydrothermal waves to exist.

The propagating waves we observe have a hydrothermal origin. The following arguments may be put forward to corroborate this proposition.

(i) In most parts of the cavity the surface velocity of the return flow is approximately the same, but the increase in wave amplitude is observed only in the region where a significant horizontal temperature gradient exists.

(ii) The waves observed are sensitive to thermal conditions on the lateral walls. Wave structures in cavities with metal and Plexiglas walls are quite different.

(iii) In the experiment we actually have a dimensionless wave number $k=2-4$. Surface waves with this k would be unstable only for a Reynolds number greater than 200 [6]. Usually the Reynolds number in our experiment is smaller than 20 when waves appear [3]. For the surface wave instability the dimensionless wave number is $k=0.1-0.2$ [6]. The wavelength in our experiment should therefore be $\lambda=30-60d$. (This length is larger than the cavity.) The surface wave mechanism must then be discarded.

Some difficulties arise when comparing our experimental results with the calculations of Smith and Davis [5,6]. These authors discuss some simplifying hypotheses which are a long way removed from the experimental situation. The main difference concerns the propagation direction of the waves, which is the opposite of that predicted in those studies.

Although we have no linear theory for these waves, we can nevertheless try to use a general nonlinear framework for propagating waves in our system. It is well known that, under very general conditions, this kind of wave can be described by a complex Ginzburg-Landau equation for the slow varying complex amplitude A of the disturbances [Eq. (1)] [14]. Taking into account the symmetries observed in the experiment one can propose an amplitude equation in the form

$$\frac{\partial A}{\partial t}=\sigma A-v_g\frac{\partial A}{\partial x}+(\beta_1+i\beta_2)\frac{\partial^2 A}{\partial x^2}+(\delta_1+i\delta_2)\frac{\partial^2 A}{\partial y^2}-(\rho_1+i\rho_2)|A|^2A. \tag{7}$$

(Notice that the term with v_g cannot be removed by Galilean variance because the boundary conditions are spatially fixed.) On the right-hand side we have a linearly unstable term, an advection term, diffusive (real part) and dispersive (imaginary part) terms, and nonlinear saturation (real part) and frequency shift (imaginary part) terms.

This equation has been used to describe, among other situations, the uniform two-dimensional flow past a symmetric body. An example of such a flow is the von Kármán vortex street behind a circular cylinder at low Reynolds numbers [15–17]. There the consequences of a Ginzburg-Landau model where the control parameter σ is spatially dependent are discussed. It is also interesting to attempt to define the nature of this instability: What conditions are necessary for convective or absolute instability? From this kind of model one can deduce that the system is convectively unstable in the range [18]

$$0<\sigma<\frac{v_g^2\beta_1}{4[\beta_1^2+\beta_2^2]}\ . \tag{8}$$

The convective character can be determined if a perturbation grows when traveling but does not saturate in the same place where it originates. Figure 6 suggests that in our system the instability is convective. We must stress that, as in the von Kármán problem, the Ginzburg-Landau equation is set as a model, but it is not deduced from hydrodynamic equations. In this experiment a detailed comparison between the basic equations and Eq. (7) is far from trivial. However, under suitable conditions, it can describe the features observed in experiments quite well.

From the results in Sec. II it is possible to estimate some coefficients in Eq. (7). The group velocity of waves and the dispersion parameter can be inferred from Eq. (6): $v_g=V+2kB$ and $\beta_2=B$. (The values of these coefficients are given in Fig. 8.) σ can be estimated from the growth rate of the amplitude along the flow where the instability begins to develop. The dependence of σ on k is shown in Fig. 10.

It is also possible to estimate the coefficient ρ_1, which is responsible for nonlinear damping of waves. Taking into consideration the results presented in Figs. 10 and 7, $\rho_1=\sigma/A_0^2$ can be calculated. We are not able to estimate the other coefficients in Eq. (7). The degree of accuracy is not sufficient to calculate ρ_2, which describes the nonlinear shift of frequency. Our impression is that ρ_2 is much smaller than ρ_1. We have no information about δ_1 and δ_2, which describe the behavior of the slowly varying amplitude in the transverse direction.

Although we do not have all the coefficients in (6), we can try to use it to explain our results concerning the

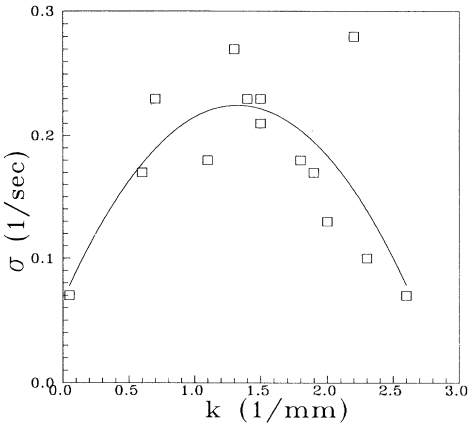

FIG. 10. Growth rate vs wave number. The growth coefficient is calculated from the fits of Fig. 6: $\sigma=(v_g/\Delta x)\ln(A_1/A_0)$. The parabola is $\sigma=0.07+0.24k-0.09k^2$.

shape of wave fronts in cavities with different walls. Studying the wave behavior we conclude that there is no indication of Eckhaus or Benjamin-Feir instability. Nor did we observe zigzag instability: It can be seen in the photographs (Fig. 3) that the wave fronts are slightly curved, but there is no periodic structure in the transverse direction.

The complex amplitude A can be written as $A=Qe^{i\phi}$. The absence of amplitude instabilities allows us to consider the case of constant Q and phase variations only. For ϕ we have

$$\phi_t'-v_g\phi_x'=\delta_1\phi_{yy}-\delta_2(\phi_y)^2 \ . \tag{9}$$

One of the steady solutions of this equation may be written as [19,20]

$$\phi(x,y)=\frac{q_++q_-}{2}y-\frac{\delta_2}{v_g}\frac{q_+^2+q_-^2}{2}x + \frac{\delta_1}{\delta_2}\ln\left[\cosh\left[\frac{\delta_2}{\delta_1}\left|\frac{q_+-q_-}{2}\right|(y-cx)\right]\right] \tag{10}$$

where $c=\delta_2(q_++q_-)/v_g$. This solution connects two branches of different inclinations

$$\phi_\pm(x,y)=q_\pm y+\frac{\delta_2}{v_g}q_\pm^2 \ . \tag{11}$$

The angles of inclination with respect to the flow velocity near the walls are

$$\tan\varphi_\pm=\frac{\delta_2}{v_g}q_\pm \ . \tag{12}$$

Using solution (11), it is possible to describe three types of patterns observed in the experiment. We obtain a wave-front structure similar to that observed in the experiment with adiabatic walls if we set $\delta_2 q_+>0, \delta_2 q_-<0$. Accordingly, for isothermal walls we set $\delta_2 q_+<0, \delta_2 q_->0$, and for the case of different walls $\delta_2 q_+<0$ (adiabatic) and $\delta_2 q_-<0$ (metallic).

It is not clear how such boundary conditions derive from the physical boundary conditions and whether another steady solutions, similar to (10), can exist. The situation here is quite similar to some experiments on wakes behind a circular cylinder [21,22]. Different shapes of the vortex behind the cylinder were observed. The axis of the vortex may be curved, and it is also possible to observe oblique shedding. As it was shown experimentally [21] it was possible to exert some control over the vortex structure behind the cylinder. This may be done by placing two cylinders with their axes perpendicular to the plane of the wake in front of the first cylinder. By changing the diameter and the distance between the control cylinders it was possible to achieve different shapes of vortex in the wake. As was pointed out [21] such an arrangement may be regarded as a definite boundary condition for the phase of the wake. These conditions seem to be very difficult to calculate from the basic equations, as are the boundary conditions for the angle of inclination of hydrothermal wave fronts in our system.

V. CONCLUSIONS

In the present paper thermal waves in a convective system with lateral heating have been described. These waves appear as perturbations superimposed on the return flow and propagate in the same direction as this flow. Their amplitude increases near the heating wall, then saturates, and later decreases. This can be explained by the nonlinearity in the surface temperature distribution and therefore by nonuniform distribution of the Marangoni number.

The spontaneous waves have frequencies in the range 1–2 Hz. They are observed in a convective (not absolute) regime. The waves are perturbed by a periodically heated wire placed near the bottom and close to the heating wall. This device makes it possible to obtain quite regular wave patterns when the frequency of this external perturbation is inside the instability range. The applied perturbation decays very rapidly, but its energy is transferred to some unstable mode that grows in some region of the container.

When using materials with different thermal properties in the bottom and in the sidewalls perpendicular to the return flow, a different curvature of the wave fronts is observed.

One of the main conclusions in this work is that the waves in question are hydrothermal waves. We discuss their structure with a Ginzburg-Landau equation. Some of the coefficients of this equation can be inferred from the experiments.

Further experiments and theoretical developments are needed to clarify and complete the description of hydrothermal waves. It would be interesting to take into account gravity effects and non-Boussinesq effects (variations of the viscosity and the thermal expansion coefficient with temperature) in theoretical analyses and in numerical simulations. The puzzling question of the

direction of propagation of waves (which is observed to be other than that predicted) still remains. From the experimental angle, the velocity profile should be measured and compared with the theoretical one. In particular, it would be interesting to determine the surface velocity and its relationship to the velocity of the waves [23]. Finally, these experiments should also be extended to low-Pr fluids (which have received ample attention in numerical and theoretical studies).

ACKNOWLEDGMENTS

We would like to thank J. Burguete, Dr. T. Ondarçuhu, and P. Elizalde for their help. This work has been supported financially by DGICYT (Spanish Government), through Contract Nos. OP90-0098 and OPB91-0627, and by the Regional Government of Navarra (Contract No. 725/91). A.B.E. also acknowledges the DGICYT for a sabbatical grant.

[1] See, for example, P. Kolodner, Phys. Rev. Lett. **66**, 1165 (1991); E. Bodenschatz, D. S. Cannell, J. R. de Bruyn, R. Ecke, Y. C. Hu, L. Lerman, and G. Ahlers, Physica D **61**, 77 (1992).

[2] D. Schwabe and L. Metzger, L. Cryst. Growth **97**, 23 (1989).

[3] A. B. Ezersky, A. Garcimartín, J. Burguete, H. L. Mancini, and C. Pérez-García, Phys. Rev. E **47**, 1126 (1993).

[4] D. Schwabe, U. Möller, J. Schneider, and A. Scharmann, Phys. Fluids A **11**, 2368 (1992).

[5] S. H. Davis, Annu. Rev. Fluid Mech. **19**, 403 (1987); M. K. Smith, J. Fluid Mech. **194**, 391 (1988); M. K. Smith, Phys. Fluids **29**, 3182 (1986).

[6] M. K. Smith and S. H. Davis, J. Fluid Mech. **132**, 119 (1983).

[7] M. Vince and M. Dubois, Europhys. Lett. **20**, 505 (1992); J. Burguete, H. L. Mancini, and C. Pérez-García, Europhys. Lett. **23**, 401 (1993). Recent experiments in this system also show hydrothermal waves.

[8] P. Huerre and P. A. Monkewitz, Annu. Rev. Fluid. Mech. **22**, 473 (1990).

[9] See, for example, D. J. Tritton, *Physical Fluid Dynamics*, 2nd ed. (Oxford, London, 1988), p. 271; Yu. S. Kachanov, V. V. Kozlov, and V. Ya. Levchenko, *The Formation of Turbulence in a Boundary Layer* (Nauka, Novosibirsk, 1982), p. 151.

[10] J. Liu and J. P. Gollub, Phys. Rev. Lett. **70**, 2289 (1993); J. Liu, J. D. Paul and J. P. Gollub, J. Fluid Mech. **250**, 69 (1993).

[11] W. Merzkirch, *Flow Visualization* (Academic, London, 1987).

[12] G. Z. Gershuni and E. M. Zhukhovitskii, *Convective Stability of Incompressible Fluids* (Keter, Jerusalem, 1976).

[13] P. Manneville, *Dissipative Structures and Weak Turbulence* (Academic, London, 1990), p. 116.

[14] P. Coullet, S. Fauve, and E. Tirapegui, J. Phys. (Paris) Lett. **46**, 787 (1985).

[15] J. M. Chomaz, P. Huerre, and L. G. Redekopp, Phys. Rev. Lett. **60**, 25 (1988).

[16] P. Albarede, M. Provansal, and L. Boyer, C. R. Acad. Sci. Paris II **310**, 459 (1990).

[17] D. S. Park and L. G. Redekopp, Phys. Fluids A **4**, 1697 (1992).

[18] R. J. Deissler, Physica D **25**, 233 (1987).

[19] A. Chiffaudel, Europhys. Lett. **18**, 589 (1992).

[20] P. Albarede and P. Monkewitz, Phys. Fluids A **4**, 744 (1992).

[21] M. Hammache and M. Gharib, Phys. Fluids A **1**, 1611 (1989).

[22] C. H. K. Williamson, J. Fluid Mech. **206**, 579 (1989).

[23] Some results have been recently published: D. Villers and J. K. Platten, J. Fluid Mech. **234**, 487 (1992).

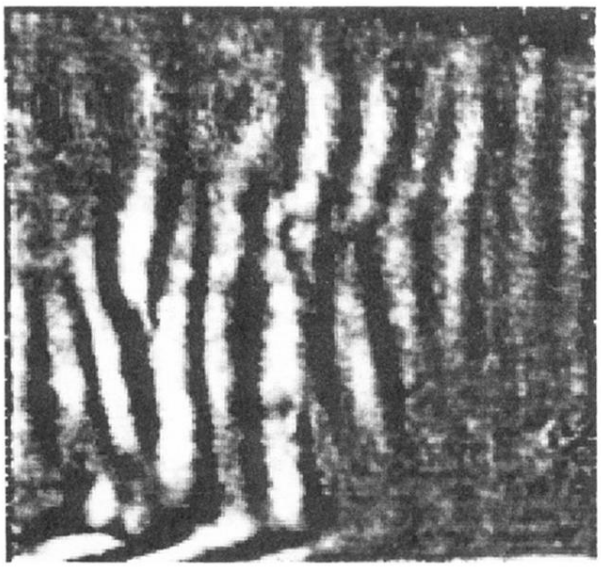

FIG. 2. Shadowgraph of hydrothermal waves. The image covers only a zone of the cavity of 3.7×3.2 cm^2.

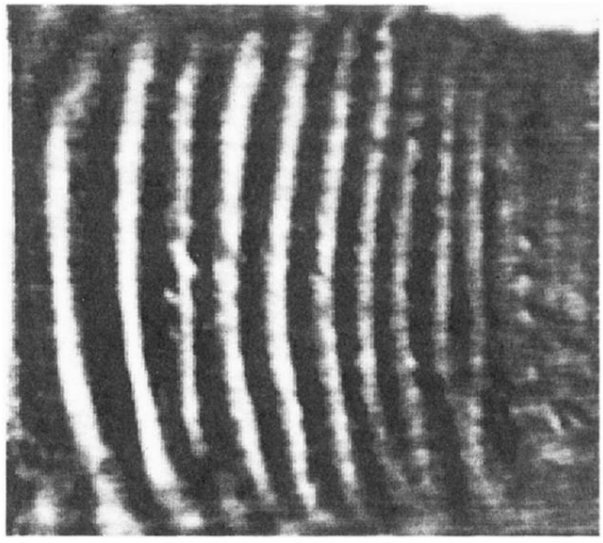

(a)

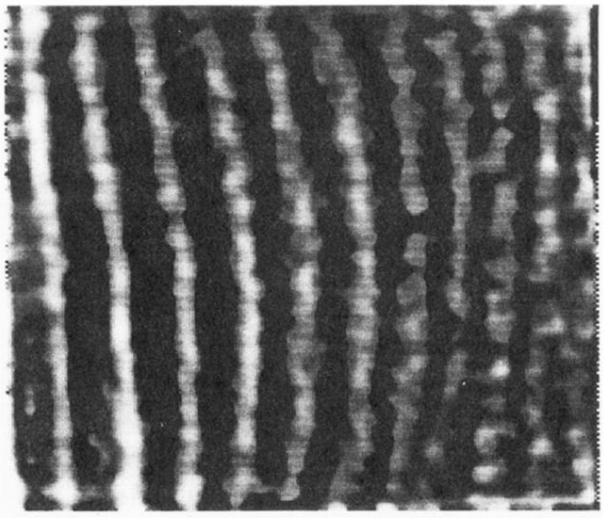

(b)

FIG. 3. Hydrothermal waves with external excitation (a) in a Plexiglas cavity and (b) in a metal cavity. The perturbation is a pulse of frequency $f_0 = 1.7$ Hz and $V = 0.3$ V. Both images display the same zone as in Fig. 2.

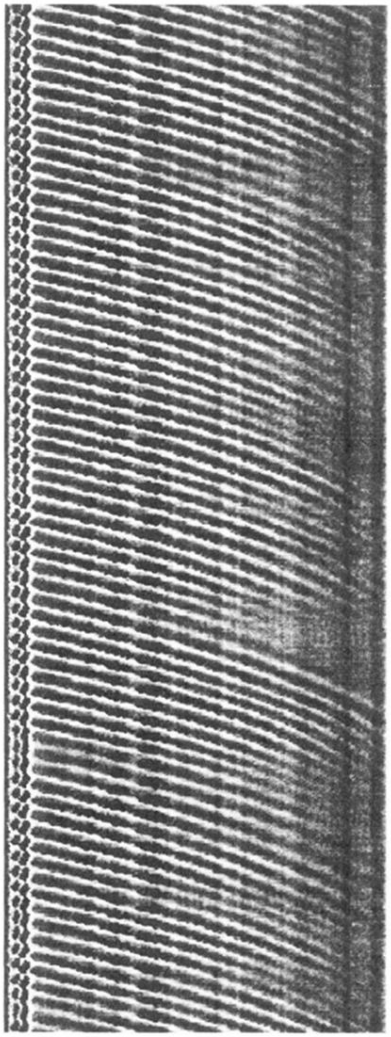

FIG. 4. *x-t* diagram obtained by recording a line of the shadowgraph image over a certain time. The horizontal axis is 3.5 cm long and the vertical axis covers 51.2 sec.

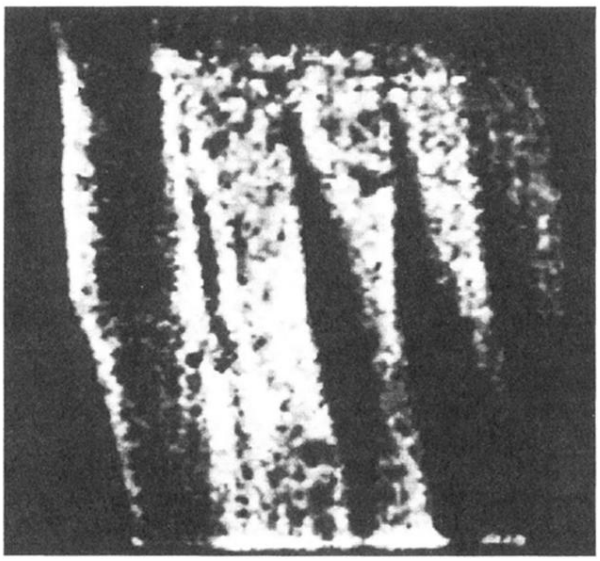

FIG. 9. Shadowgraph of hydrothermal waves in a cavity with one metal wall and one wall of Plexiglas. The area covered by the photograph is 3.7×3.2 cm^2.